

Identifying a Transition Climate Zone in an Arid River Basin using a Hydrological Drought Index

Libo Zhang¹, Yongqiang Liu², Lu Hao¹, Decheng Zhou¹, Cen Pan¹, Peilong Liu¹, Zhe Xiong³, Ge Sun⁴

¹Jiangsu Key Laboratory of Agricultural Meteorology, International Center for Meteorology, Ecology, and Environment, College of Applied Meteorology, Nanjing University of Information Science and Technology, Nanjing, China

²Center for Forest Disturbance Science, USDA Forest Service, Athens, Georgia, USA

³Institute of Atmospheric Physics, Chinese Academy of Sciences, Beijing, China

⁴Eastern Forest Environmental Threat Assessment Center, USDA Forest Service, Raleigh, North Carolina, USA

Correspondence to: Yongqiang Liu (yliu@fs.fed.us)

Abstract. Drought indices have been widely used in climate classification. However, there is not enough evidence for their ability in identifying the multiple climate types in areas with complex topography and landscape, especially in those areas with a transition climate. This study compares a meteorological drought index, the aridity index (AI) defined as the ratio of precipitation (P) to potential evapotranspiration (PET), with a hydrological drought index, the evaporative stress index (ESI) defined as the ratio of actual evapotranspiration (AET) to PET . We conducted this study using modeled high resolution climate data for period of 1980-2010 in the Heihe River Basin (HRB) in the arid northwestern China. PET was estimated using the Penman-Monteith and Hamon methods. The climate classified by AI shows two distinct climate types for the upper and the middle and lower basin reaches, while three types were found if ESI was used. This difference indicates that only ESI is able to identify a transition climate zone in the middle basin. This contrast between the two indices is also seen in the inter-annual variability and extreme dry / wet events. The magnitude of variability in the middle basin is close to that in the lower basin for AI , but different for ESI . AI has larger magnitude of the relative inter-annual variability and greater decreasing rate from 1980-2010 than ESI , suggesting the role of local hydrological processes in moderating extreme climate events. Thus, the hydrological drought index is better than the meteorological drought index for climate classification in the arid Heihe River Basin where local climate is largely determined by topography and landscape. We conclude that the land-

surface processes and human disturbances play an important role in altering hydrological drought conditions and their spatial and temporal variability.

1 Introduction

Large river basins at continental and sub-continental scales usually encompass multiple climate types related to complex topography and landscape. Climate is more humid in the upper basin near the river origins with high elevations and forest and / or permanent snow cover than the lower basin with low elevations and less vegetated lands. Climate could be extremely dry in parts of a watershed under a prevailing atmospheric high pressure system. The sub-continental Colorado River watershed, for example, is dominated by cold and humid continental climate in the upper basin of the Rocky Mountains and cold semi-arid or warm desert climate in the lower basin of the southern inter-mountains.

This feature of multiple climate types is also seen in some smaller basins. The Heihe River Basin (HRB) in northwestern China, for example, has an area of 130, 000 km² with annual precipitation varying dramatically from about 500 mm in the upper basin of the Qilian Mountains with forest-meadow-ice covers in the south to less than 100 mm in the lower basin of the Alxa High Plain with Gobi and sandy lands in the north. Climate types change from cold and humid continental to arid desert, accordingly.

The relative high precipitation in the humid upper basin supports forests and meadows and provides source water lower reaches of the Heihe River. In contrast, water is a major limitation factor in arid lower basin. In addition, more extreme weather conditions, especially droughts, occur in arid lower basin. In the Colorado River basins, the reconstructed data show decadal periods of persistently low flows during the past centuries (Woodhouse et al., 2010). The drought severity in the new millennia has been the most extreme over a century (Cayan et al., 2010). The reconstructed precipitation series in the HRB indicates that droughts were much more frequent and lasted longer than floods in the past two centuries (Ren et al., 2010). Droughts occurred more often in the dry lower basin than the humid upper basin (Li, 2012).

The watersheds with varied topography and landscape may have a transition climate zone between the two zones. In the HRB, for example, the Koppen climate classification (Peel et al., 2007) shows polar tundra or boreal climate in the upper basin of the mountain regions in

the south, arid desert climate in the lower basin in the north, and a transition zone of steppe climate in the middle. Identifying this transition zone and understanding its unique climate features are of both scientific and management significance. The complex topography in upper basin and harsh climate in lower basin make both regions unsuitable for human living. The transition zone however is relatively flat in comparison with the mountain region and less arid in comparison with the dryland region. It therefore provides a favorable condition for industrial and agricultural development. Also, the environmental conditions in this region are more dynamical and localized because of human induced rapid and fragmental landscape changes.

The Koppen climate classification, one of the most widely used climate classification techniques at large geographic scales and constructed based on the properties of ecosystems, latitude, and average and seasonal precipitation and temperature, is often used for a large region with static environmental conditions. Drought indices are another useful tool to classify and monitor aridity and drought of a region. Drought indices are quantitative measures of drought levels by combining one or several variables (indicators) into a single numerical value (Zargar et al., 2011). Drought indices are usually categorized into meteorological, hydrological, agricultural, and social droughts (Wilhite and Glantz, 1985). Different definitions can be found. The first two types of droughts investigated in this study were simply considered as a lack of water due to anomalous atmospheric and land-surface conditions, respectively.

Precipitation, temperature and humidity are atmospheric conditions often used to estimate meteorological drought indices. Percent of Normal (PN) and Standardized Precipitation Index (SPI) (McKee et al., 1993) are simply based on precipitation and can be used to measure anomalies of a period over various lengths. Palmer Drought Severity Index (PDSI) (Palmer, 1965) and Keetch-Byram Index model (Keetch and Byram, 1968) are based on water supply and demand estimated mainly using precipitation and temperature (Guttman, 1999). Both indices depend on precedent daily or monthly values, making them specifically useful for a persistent event like drought. The aridity index (AI) (Budyko, 1974) uses annual averages of precipitation and potential evapotranspiration (PET), which is mainly determined by temperature. AI is also used as an essential element in many other indices to describe actual drought conditions (Arora, 2002). Different from the above four indices, which are

often used to indicate the dry spells of temporal humidity variability, AI is often used to indicate a climatic humidity condition of a region.

Land-surface conditions are streamflow, runoff, actual evapotranspiration, etc. Streamflow Drought Index (SDI) (Nalbantis and Tsakiris, 2009) and Surface Water Supply Index (SWSI) (Shafer and Dezma, 1982) use streamflow as well as reservoir storage and precipitation to monitor abnormal surface water (Narasimhan and Srinivasan, 2005). Standardize Runoff Index (SRI) (Shukla and Wood, 2008) is standard normal deviate associated with runoff accumulated over a specific duration. Evaporative Stress Index (ESI) defines dryness degree based on the ratio of actual evapotranspiration (AET) to PET. A relatively low ESI indicates water limitation to plants and the actual rate is way below the PET. In contrast, a relatively high ESI indicates freely available water with the AET rate approaching or close to the PET. The ESI has been long used to evaluate the irrigation need for crop growth and land classification (Yao, 1974). The ESI has been used recently to evaluate water stress using remotely sensed hydrological and ecological properties (Anderson et al., 2016).

Many studies have compared various types of drought indices in different climatic environments. Otkin et al. (2013) compared the ESI with drought classification used by the U.S. Drought Monitor (USDM) (Svoboda et al., 2002) and found that the ESI anomalies led the USDM drought depiction by several weeks and large ESI anomalies therefore were indicative of rapidly drying conditions. This finding was coincident with the droughts occurred across the United States in recent years. Choi et al. (2013) compared the ESI with the Palmer drought severity index (PDSI) in a watershed of the Savannah River branch in southeastern United States during 2000-2008. They found that the ability of the ESI to capture shorter term droughts was equal or superior to the PDSI when characterizing droughts for the watershed with a relatively flat topography dominated by a single land cover type. However, the differences between the meteorological and hydrological drought indices in capturing the spatial patterns and temporal variations under complex topography and environments, especially with a transition zone, are not well characterized and understood.

This study is to understand the capacity a meteorological drought index, AI, and a hydrological drought index, ESI, in identifying the transition climate zone in the HRB. It was made mainly by comparing the spatial patterns and regional averages. Their temporal variations were also analyzed to understand the differences in the seasonal and inter-annual

variability and long-term between the meteorological and hydrological drought indices. The data from a high-resolution regional climate modeling were used.

2 Methods

2.1 Study region

The study region was the HRB and the adjacent areas (Fig. 1). The Heihe River originates from the Qilian Mountains in the northern edge of the Tibet Plateau and flows northward to the China-Russian border. The HRB spans between 98°~101°30'E and 38°~42°N. The upper HRB is within the mountains elevated 2300~3200m mainly covered with forests and mountain meadows. The middle HRB is along the Hexi Corridor elevated 1600~2300m mainly covered with piedmont steppe grass, crops, and residence and commercial uses. The lower HRB is in the Alxa High-Plain elevated below 1600m mainly covered with Gobi and desert sands.

Annual precipitation is over 400mm in the upper basin, with the maximum of 800mm at extremely high elevations, about 100~250mm in the middle basin, and below 50mm in many lower basin areas. The annual precipitation in the upper basin has high seasonal variability, and nearly 70% of the total annual rainfall occurs from May to September (Gao et al., 2016). The upper basin generates nearly 70% of the total river runoff, which supplies agricultural irrigation and benefits the social economy development in the middle and lower basin reaches (Yang et al., 2015; Chen et al., 2005). Annual mean temperature is about -4°C in the upper basin, 7°C in the middle basin, and nearly 9°C in the lower basin.

2.2 Drought indices

The meteorological drought index is defined as $AI = P / PET$, where P and PET are daily precipitation and potential evapotranspiration, respectively. AI is a variant of the index originally defined by Budyko (1974), which is the ratio of annual PET to P . The average AI values were used to classify the arid, semi-arid, semi-humid (sub-humid), and humid climate with the ranges of $AI \leq 0.2$, $0.2 < AI \leq 0.5$, $0.5 < AI \leq 1.3$, and $AI > 1.3$, respectively (Ponce et al., 2000).

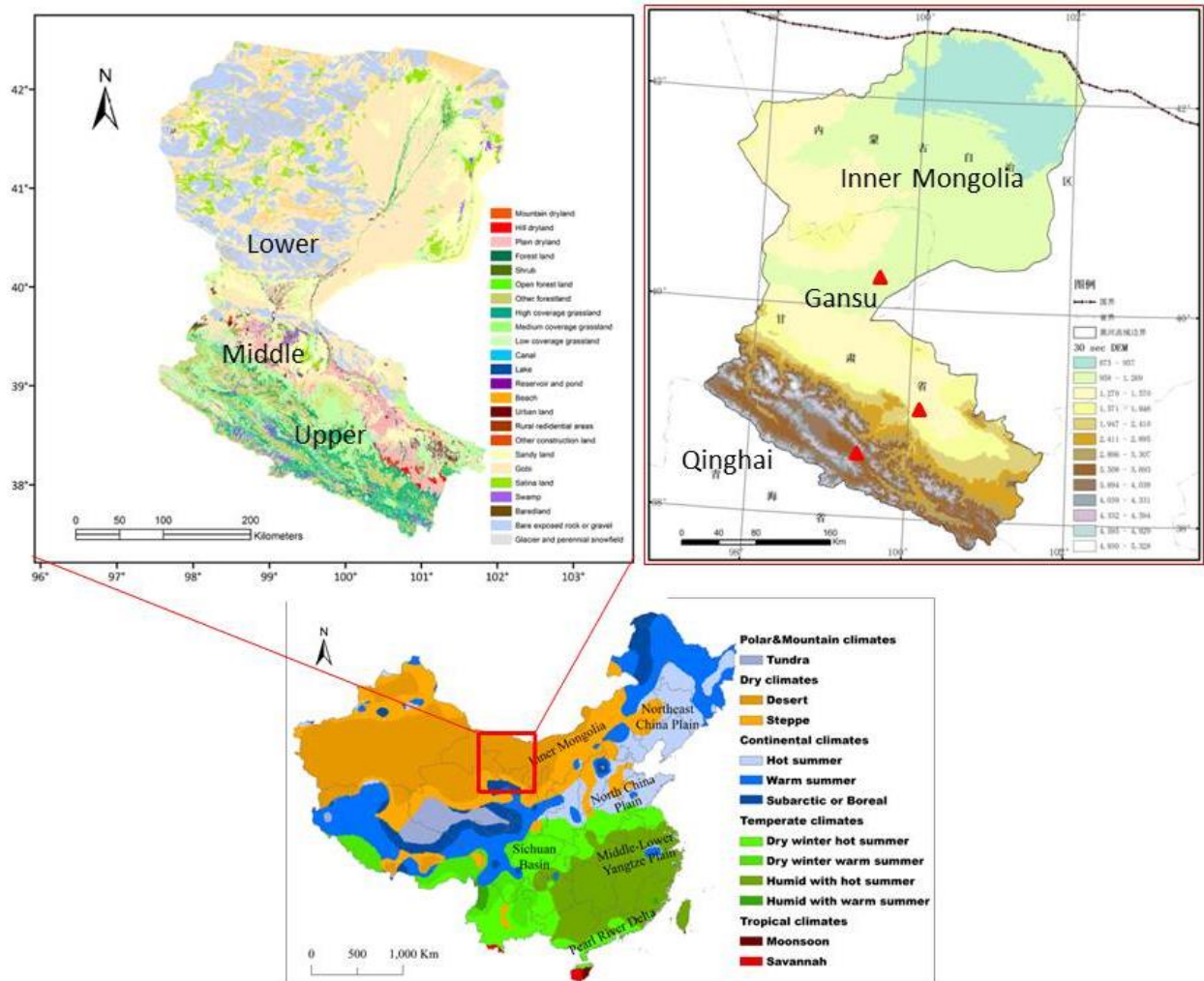


Figure 1. The study region of the Heihe River Basin, with landscape (upper left) and elevation (meter) and three provinces (upper right) (data source: Wang et al., 2014). The triangles signs in upper left are meteorological observation sites. The bottom panel shows the location of the study region in China and the Koppen climate classification (from Peel et al., 2007).

The hydrological drought index is defined as $ESI = AET / PET$, where AET is daily actual evapotranspiration. The ranges of average ESI values of $ESI \leq 0.1$, $0.1 < ESI \leq 0.3$, $0.3 < ESI \leq 0.6$, and $ESI > 0.6$ were used to classify the arid, semi-arid, semi-humid, and humid climate, respectively (Yang, 2007). This approach agrees with Anderson (2011), which showed that the ESI values varying gradually from 0 to 1 correspond to several USDM drought levels

from exceptional to no drought for each month from April to September across the continental U.S.

Two methods were used to estimate *PET* (mm/d). One was the energy balance based FAO-56 Penman-Monteith Equation (Allen et al. 1998):

$$PET_p = \frac{0.408\Delta(R_n - G) + \gamma \frac{900}{T+273} u_2 (e_s - e)}{\Delta + \gamma(1 + 0.34u_2)} \quad (1)$$

where R_n and G are net radiation and soil flux on the ground ($\text{MJm}^{-2}\text{d}^{-1}$); T is air temperature ($^{\circ}\text{C}$); e_s and e are saturation and actual water vapor pressure (kPa); u_2 is wind speed at 2m above the ground (ms^{-1}); Δ is the rate of change of e_s with respect to T ($\text{kPa}/^{\circ}\text{C}$); γ is the psychrometric constant ($\text{kPa}/^{\circ}\text{C}$). The other method is the temperature based on Hamon formula (Hamon, 1963):

$$PET_h = \frac{k \times 0.165 \times 216.7 \times N \times e_s}{T + 273.3} \quad (2)$$

where k is proportionality coefficient = 1; N is daytime length. e_s is in 100 Pa here.

Monthly *PET*, precipitation and actual evapotranspiration, obtained based on daily values, were used to calculate the drought indices. It was assumed that daily *PET*=0 if daily $T < 0^{\circ}\text{C}$. Their monthly *PET* was not used if *PET*=0 for more than 10 days in a month. In this case, no drought indices were calculated for the month. It was also assumed that daily ground energy was in balance, so $R_n - G = H + L \times AET$, where H and L are sensible heat flux and potential heat constant.

The data used in calculation and evaluation of the drought indices are listed in Table 1.

Table 1. The data used in calculation and evaluation of the drought indices. H , AET , P , T , and e (RH) are sensible heat flux, actual evapotranspiration, precipitation, temperature, wind speed, and water vapor pressure (relative humidity). HRB stands for Heihe River Basin.

Source	Parameter	Time Period	Space	Reference
Simulation	H , AET , P , T , u , e	1980-2010, daily	HRB, 3 km resolution	Xiong and Yan (2013)
Observation	P , T , RH	1980-2010, daily	3 sites in HRB	China National Met Sci Infrastructure (data.cma.cn)

2.3 Regional climate modeling

The climatic and hydrological data used to calculate the drought indices were created from a regional climate modeling using the Regional Integrated Environmental Model System (RIEMS 2.0) (Xiong and Yan, 2013). The simulation was conducted over the period of 1980-2010. The horizontal spatial resolution was 3km. A unique feature with this simulation was that the model's parameters, including soil hydrological properties, were recalibrated based on observations and remote sensing data over the HRB that greatly improved the model's performance. The model evaluation indicated that the model was able to reproduce the spatial pattern and seasonal cycle of precipitation and surface T . The correlation coefficients between the simulated and observed pentad P were 0.81, 0.51, and 0.7 in the upper, middle, and lower HRB regions, respectively ($p < 0.01$).

The historical T and P observations during the simulation period at Yeilangou of the upper basin (38.25°N, 99.35°E, 3300m above the sea level), Zhangye of the middle basin (38.11°N, 100.15°E, 1484m), and Dingqing of the lower basin (40.3°N, 99.52°E, 1177m) (Fig. 1) were used to compare with the simulations.

3 Results

3.1 Simulated climate and hydrology

The spatial pattern of the simulated annual T averaged over the simulation period is featured by the large changes between basin reaches, increasing from about -15°C in the tall mountains of the upper basin to over 10°C in the deserts of the lower basin (Fig. S1). The simulated average annual P shows an opposite gradient, decreasing from about 2.5 mm/d in the mountains to less than 0.25 mm/d in the deserts (Fig. S2). The simulated average annual AET has a similar pattern to precipitation (Fig. S3). The spatial variability is much larger within the upper basin than the lower basin.

An interesting feature is that both T and P in the middle basin are very close to their corresponding values in the lower basin but much different from those in the upper basin; the AET difference between the middle and upper basin reaches however is much small.

As expected, the regional AET values averaged over the simulation period are higher in summer than in winter (Fig. S4). In the upper basin, for example, T increases from about -15°C in winter to 10°C in summer, P increased from about 0.25 to 4 mm/d, and AET from

about 0.25 to 2.5 mm/d. Again, T and P are close between the middle and lower basin reaches all seasons, and AET is close between the middle and upper basin reaches during winter and spring. While AET is close between the middle and lower basin reaches during summer and fall, the differences between the middle and upper basin reaches are much smaller than the differences in T or P .

The inter-annual variability of regional T and P is similar between the middle and lower basin reaches (Fig. S5). A few dry years (e.g., 1990, 2001, and 2008) and wet years (e.g., 1981, 1989, 2002, and 2007) can be found. The amplitude of variability is larger for P than T , especially in the upper basin. The variability of AET is also similar between the lower and middle basin reaches, but it differs from that in the upper basin during some periods (e.g., around 1985). The differences in AET between the middle and upper basins are much smaller in the magnitude than those for the meteorological properties.

The above features of close values and similar inter-annual variability in the simulated T and P between the middle and lower basin reaches are also seen in the observations (Fig. S6). The simulated T in all basin regions and P in the middle and lower basin reaches are close to the observed ones. However, the simulated P is about 0.4 mm/d higher (about 1.6 mm/d for simulation vs. 1.2 mm/d for observation). The weather site in the upper basin is located in relatively flat and low valley, while the simulation grids have many points at high elevations where P is larger than at the valley locations.

The simulated P increases around 50% over the simulation period, statistically significant at $p < 0.01$ in all basin reaches (Table S1). The simulated AET also increases, but at a smaller degree of around 20% and $p < 0.01$ only in the upper basin. The simulated T shows increasing trends, but insignificant in all reaches. The simulated P trends are close to the observed ones in the middle and lower basin reaches, but opposite to that in the upper basin. The simulated T underestimates the observed warming, which was about 2°C at $p < 0.01$.

3.2 Spatial patterns of drought indices

PET calculated using the Penman-Monteith method is mostly 1.7-2.25 mm/d in the upper basin (Fig. 2). It increases to above 3 mm/d in the middle and lower basins. There is little difference between the two regions. The meteorological drought index, AI , shows a similar pattern but opposite gradient (Fig. 3). It is as large as 1.4 in the upper basin, but reduced to

less than 0.2 in two other basin regions, indicating increasing aridity from the upper to lower basin. The hydrological drought index, *ESI*, has the same gradient as *AI*, but with different spatial pattern (Fig. 4). It is as high as 0.9 in the upper basin and reduced to mostly below 0.1 in the lower basin. However, the values in the middle basin is as high as 0.6, much larger than that in the lower basin.

P and *AET* are the highest in the upper basin and the lowest in the lower basin, while *T* and *PET* have an opposite seasonal cycle. This explains why *AI* and *ESI* are larger in the upper basin than the middle or lower basin.

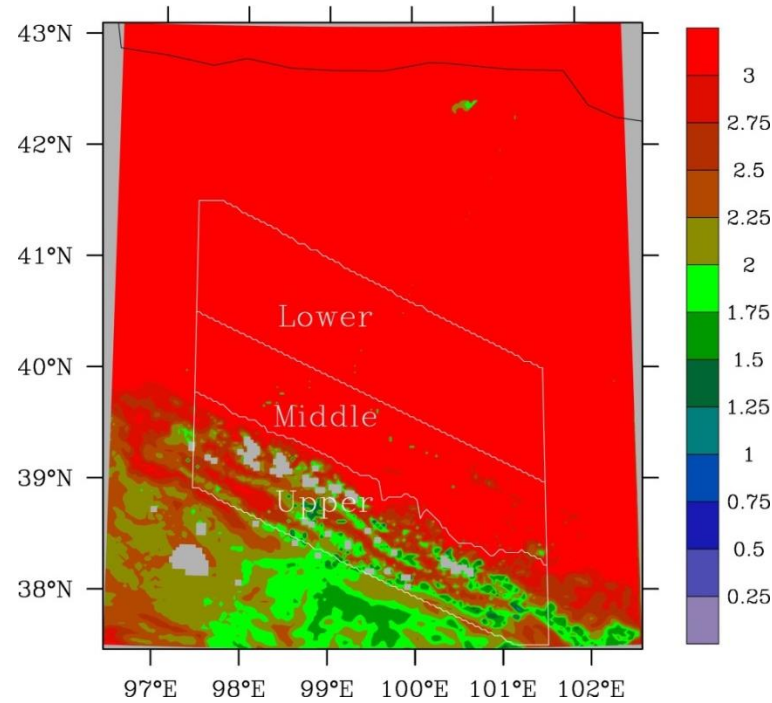


Figure 2. Spatial distributions of potential evapotranspiration (*PET*, mm/d) estimated using the Penman-Monteith method.

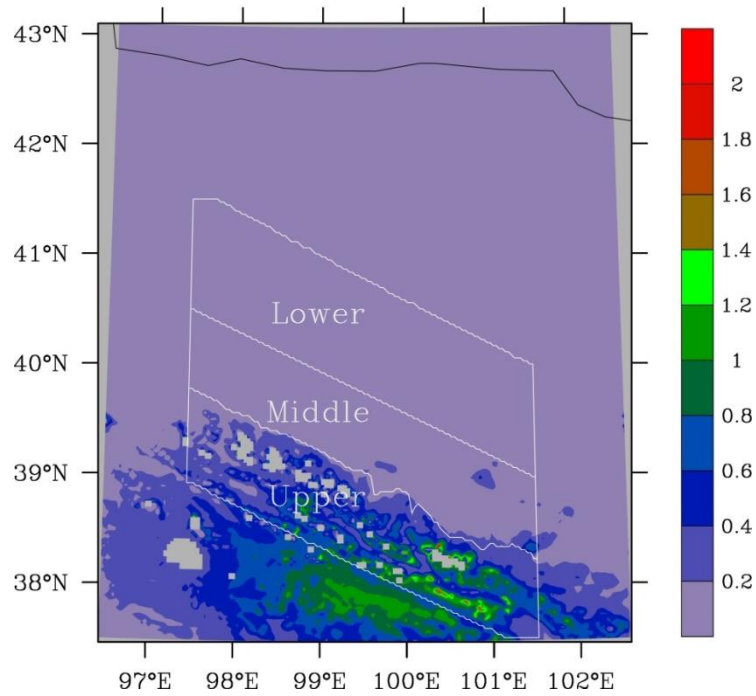


Figure 3. Spatial distributions of aridity index with potential evapotranspiration estimated using the Penman-Monteith method.

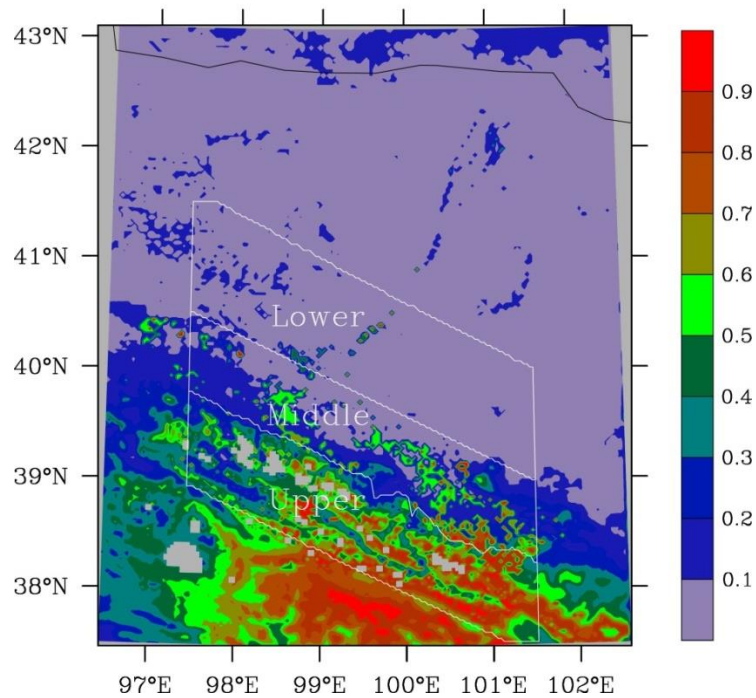


Figure 4. Spatial distributions of evaporative stress index with potential evapotranspiration estimated using the Penman-Monteith method.

PET calculated using the Hamon method has the same pattern as the one using the Penman-Monteith method, but with smaller magnitude (Fig. 5). *PET* is mostly about 1 mm/d in the upper basin and increases to about 1.5-1.75 mm/d in the middle basin, and further to 1.75-2.25 mm/d in the lower basin.

The different spatial patterns between *AI* and *ESI* seen above are also found for the Homan method. *AI* is mostly above 0.6 in the upper basin (Fig. 6). It is below 0.2 in the middle and lower basins without apparent differences between the two regions. In contrast, while *ESI* remains large values of mostly above 0.9 in the upper basin and low values of below 0.2 in the lower basin, the values in many areas of the middle basin are 0.4-0.9, much different from those in the lower basin (Fig. 7).

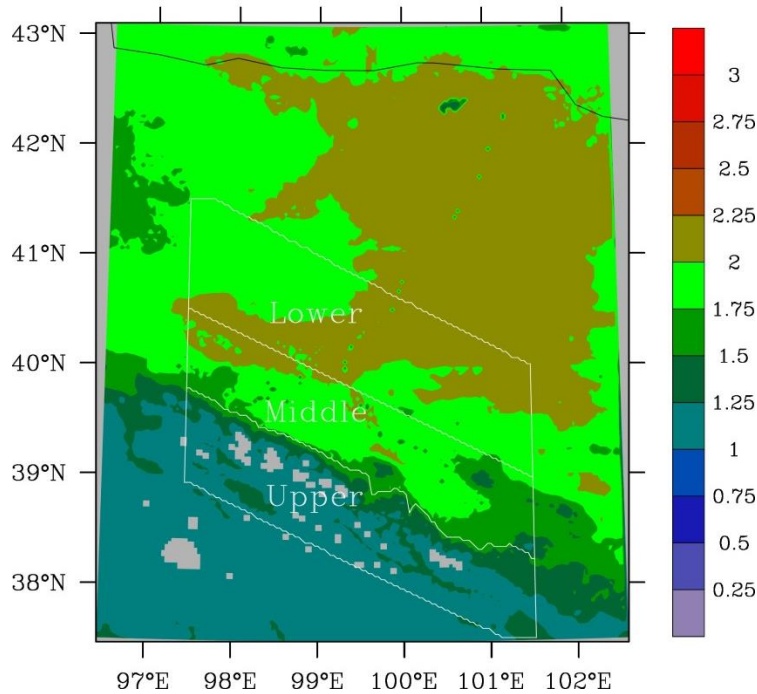


Figure 5. Spatial distributions of potential evapotranspiration (*PET*, mm/d) estimated using the Hamon method.

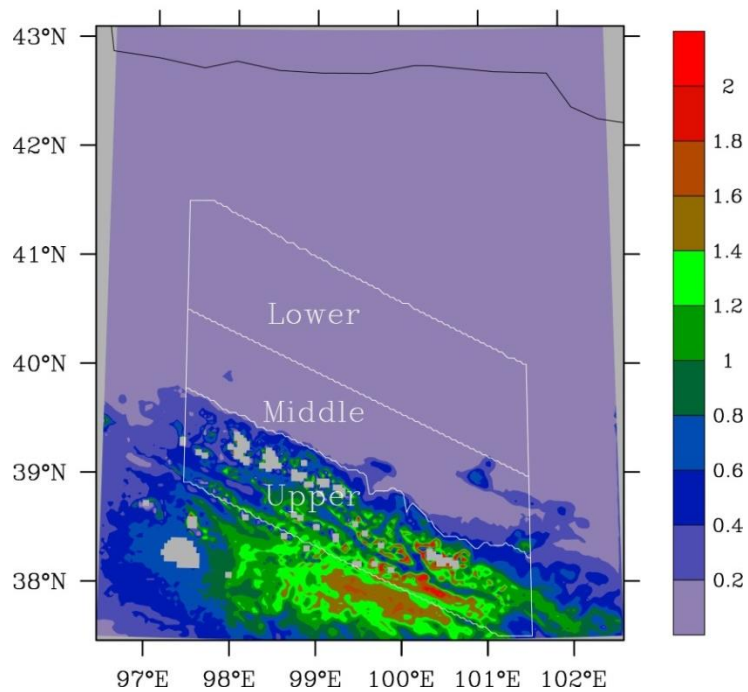


Figure 6. Spatial distributions of aridity index with potential evapotranspiration estimated using the Hamon method.

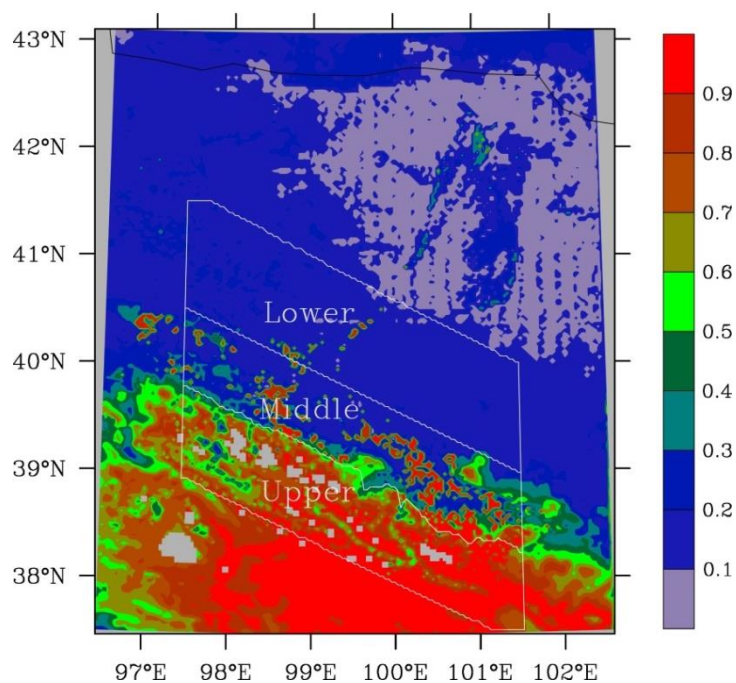


Figure 7. Spatial distributions of evaporative stress index with potential evapotranspiration estimated using the Hamon method.

3.3 Climate classification

The annual *PET* averages over 1980-2010 calculated using the Penman method are 2.12, 3.91, and 4.76 (Table 2 and Fig. 8). The corresponding *AI* values are about 0.9, 0.12, and 0.04, falling into semi-humid, arid, and arid climate. The corresponding *ESI* values are 0.63, 0.22, and 0.07, falling into humid, semi-arid, and arid climate. The annual *PET* averaged over 1980-2010 calculated using the Homan method are 1.25, 2.33, and 2.65 mm/d for the upper, middle, and lower basin reaches. The corresponding *AI* values are about 1.3, 0.18, and 0.07, falling into humid, arid, and arid climate. The corresponding *ESI* values are 0.78, 0.31, and 0.13, falling into humid, semi-humid, and semi-arid climate.

Thus, the climate across the HRB classified using *AI* has two types of semi-humid (the Penman method for *PET*) or humid (the Homan method) in the upper basin, and arid in both middle and lower basin reaches. In contrast, the climate classified using *ESI* has three types of humid in the upper basin, semi-arid (the Penman method) or semi-humid (the Homan method) in the middle basin, and arid (the Penman method) or semi-arid (the Homan method) in the lower basin. This indicates that only the hydrological drought index is able to identify the transition climate zone in the middle basin.

The difference between *AI* and *ESI* in classifying climate is related to the similar feature with the meteorological variables. Annual *P* is 555 mm in the upper basin, which is substantially different from 69-139 mm in the middle and lower basins. The mean *T* is -4.0°C in the upper basin, which is well below 6.9-8.7°C in the middle and lower basin reaches. The corresponding *PET* values fall into two groups, 299 mm in the upper basin and 672-767 mm in the middle and lower basin reaches. This explains why the *AI* falls into two groups. In contrast, *AET* is 226, 161, and 80 mm, substantially different not only between the middle and upper reaches but also between the middle and lower reaches. This explains why the *ESI* falls into three groups.

Table 2. Regional average (AVE), standard deviation (SD), and coefficient of variation (CV) for potential evapotranspiration (*PET*, mm/d), aridity index (*AI*), and evaporative stress index (*ESI*).

PET	Basin	PET			AI			ESI		
		AVE	SD	CV	AVE	SD	CV	AVE	SD	CV
Penman-Monteith	Upper	2.12	0.12	0.06	0.90	0.32	0.35	0.62	0.07	0.11
	Middle	3.91	0.21	0.05	0.12	0.06	0.50	0.22	0.06	0.26
	Lower	4.76	0.29	0.06	0.04	0.03	0.64	0.07	0.03	0.41
Hamon	Upper	1.25	0.04	0.03	1.30	0.37	0.29	0.78	0.05	0.07
	Middle	2.33	0.11	0.05	0.18	0.08	0.43	0.31	0.06	0.19
	Lower	2.65	0.16	0.06	0.07	0.04	0.56	0.13	0.04	0.31

3.4 Temporal variations of drought indices

3.4.1 Seasonal cycle

For the Penman-Monteith method, *PET* is the highest in summer and smallest in winter (Fig. 8). Note that winter *PET* in the upper basin is not shown because *T* is below zero in too many days. The amplitude in the middle basin is close to that in the lower basin, but much larger than that in the upper basin. Different from the upper basin where *AI* and *ESI* are also the largest in summer, *AI* is the largest in fall, while *ESI* is the largest in winter in the middle basin (as well as lower basin). The seasonal variations of *PET*, *AI* and *ESI* estimated using the Homan method are similar to those using the Penman method.

The seasonal *AI* and *ESI* cycles are related to those of the meteorological and hydrological conditions. *T*, *P* and *AET* (Fig. S4), and *PET* (Fig. 8) all increase from winter to summer. In the upper basin, the increases in *P* and *AET* from spring / fall to summer are larger than the corresponding increases in *PET*, leading to larger *AI* and *ESI* values in summer. In the middle as well as lower basin, however, *PET* increases substantially from spring / fall, leading to smaller *AI* and *ESI* in summer than in spring / fall.

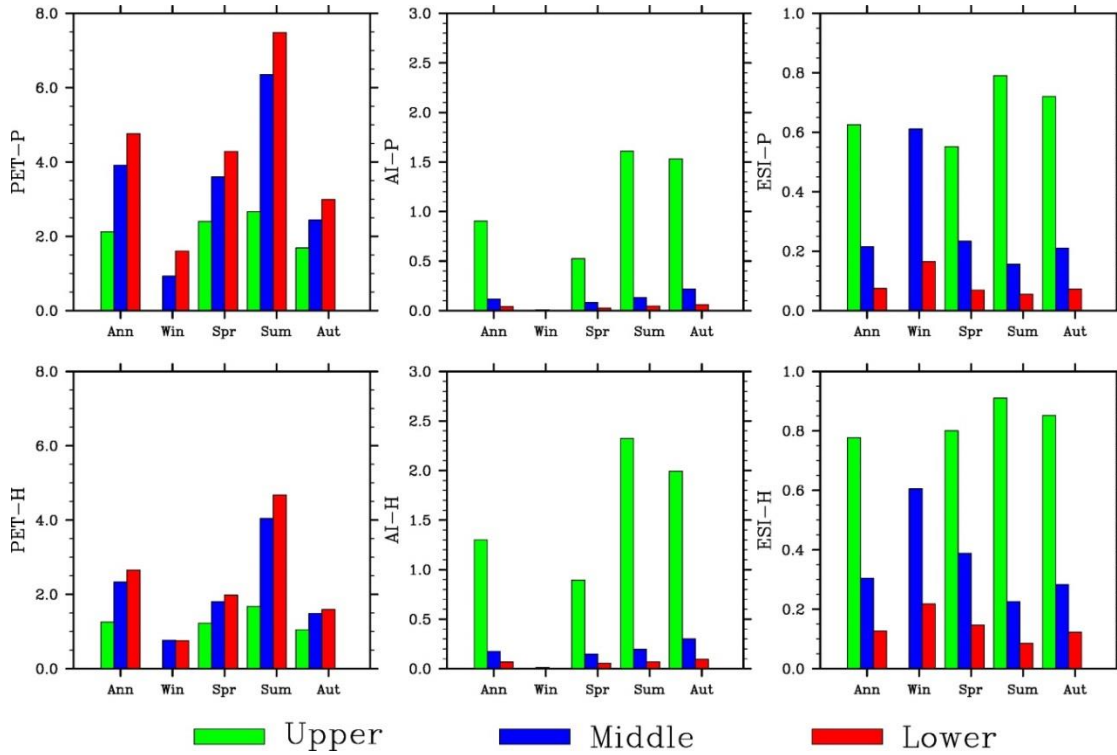


Figure 8. Seasonal variations of simulated potential evapotranspiration (PET , mm/d), aridity index (AI), and evaporative stress index (ESI) (from left to right). The top and bottom panels are for the Penman-Monteith and Hamon method, respectively.

3.4.2 Inter-annual variability

PET in the middle basin calculated using the Penman-Monteith method shows similar inter-annual variability over the period of 1980-2010 to that in the lower basin, but much different from that in the upper basin (Fig. 9). The standard deviation (SD) increases from the upper (0.12) to middle (0.21) and to lower basin (0.29) (Table 2). The coefficient of variation (CV) (the ratio of the standard deviation to the average), a statistical property often used to measure relative variability intensity, however, is comparative among the reaches.

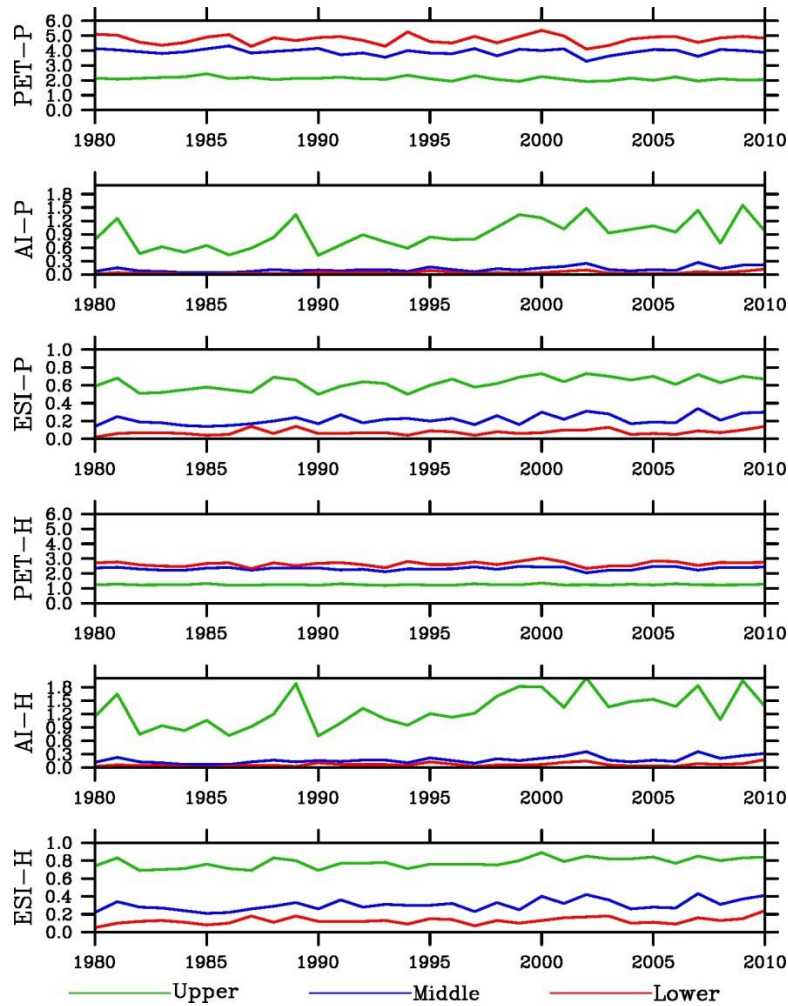


Figure 9. Inter-annual variations of potential evapotranspiration (PET , mm/d), aridity index (AI), and evaporative stress index (ESI). P and H indicates the Penman-Monteith and Hamon method, respectively.

The SD values of both AI and ESI decrease from the upper to middle and to lower basin. However, SD of AI (ESI) in the middle basin is much closer to that in the lower (upper) basin. The CV values have opposite gradient to SD, increasing from the upper to middle and to lower basin. In addition, CV differs mainly not between the basin reaches but between drought indices: AI is larger than ESI .

3.4.3 Long-term trends

PET shows little trends over the simulation period (Table 3). In contrast, drought indices increased dramatically, by 60% or more for *AI* and 15-50% for *ESI*. The trends are significant at $p<0.01$ in the upper and middle basin reaches and $p<0.05$ in the lower basin. The results indicate a less dryness condition in the HRB, which is the more remarkable in the middle than upper basin and in the meteorological than hydrological drought index. Increase in precipitation is a major contributor.

Table 3. Mann-Kendall trends from 1980 to 2010 of potential evapotranspiration (*PET*), aridity index (*AI*), and evaporative stress index (*ESI*) (in%). P (H) indicates the Penman-Monteith (Hamon) method. The bold and italic numbers are significant at $p<0.01$ and $p<0.05$, respectively.

Index	Upper	Middle	Lower
PET-P	-7.3	-2.7	0.3
AI-P	72.5	98.6	<i>80.9</i>
ESI-P	24.8	51.4	<i>47.8</i>
PET-H	0.0	2.7	3.6
AI-H	62.6	84.3	<i>66.3</i>
ESI-H	16.2	40.8	<i>40.5</i>

3.5 Extreme events

The drought indices for 4 simulated dry years (1982, 1990, 2001, and 2008) and 4 wet years (1981, 1989, 2002, and 2007) (Figs.S7-8) and the averages over the dry or wet years (Fig. 10) were analyzed. The annual *AI* values using the Penman-Monteith method are 0.4-0.5 for the first two dry years and 0.7-1.0 for the last two years in the upper valley (Fig. 10). The average over the 4 years is about 0.65. In comparison, the average is about 0.9 over 1980-2010 and 1.4 over the 4 wet years. The values are very small in spring (except in 1982) and occasionally in fall (1990). The annual *AI* values in the middle and lower basin reaches are below 0.2 for individual dry years and average. The small values are found for individual seasons except falls of the last two years in the middle basin. In comparison, the annual values are 0.4 or above in 3 falls of the 4 wet years.

The annual *ESI* values using the Penman-Monteith method are 0.5 or larger in the upper valley. The average over the 4 years are nearly 0.6. In comparison, the average is about 0.62

over 1980-2010 and 0.7 over the 4 wet years. The values are comparable from spring to fall, though relatively smaller in spring. This is different from AI. The annual *ESI* values are about 0.2 in the middle and below 0.1 in the lower basin for individual dry years and average. Thus, the values are apparently different between the middle and lower basin reaches. This is another difference from AI. The lowest values mostly occur in summer in both basin reaches. In comparison, the annual values are 0.25-0.35 in the middle basin and 0.1 or larger in 3 of the 4 wet years in the lower basin.

Same results, that is, substantially smaller *AI* than normal, especially in spring but no much *ESI* changes from normal and between seasons in the upper basin, and no much *AI* change from normal and wet events (small in all cases) in the middle and lower basin reaches but much smaller *ESI* than wet events and different between the two basin reaches, can be found for the Hamon method, though slightly larger *AI* and *ESI* values. The results suggest that *ESI* is better representative of extreme dry conditions in the middle basin, but less sensitive to drought in the upper basin.

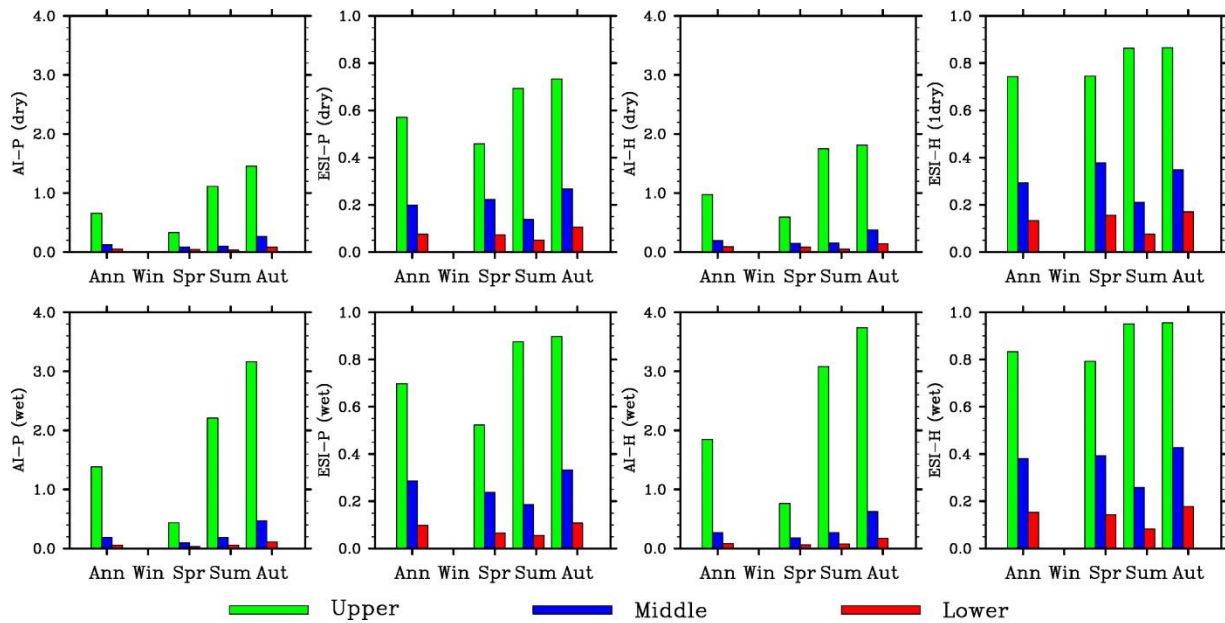


Figure 10. Seasonal variations of simulated aridity index (*AI*), and evaporative stress index (*ESI*) using the Penman-Monteith and Hamon methods (left to right) for averages over the dry years of 1982, 1990, 2001, 2008 (top) and (bottom).

4 Discussion

4.1 Supports to the integrated water–ecosystem–economy study in the HRB

The HRB is a typical inland river basin with a strong contrast in topography, landscape, climate, and human activities from the headwater to end point along its drainage system. Comprehensive monitoring, modeling, and data manipulation studies have been conducted for several decades to understand the hydrological and ecological processes and interactions in the HRB (Cheng et al., 2014). The middle HRB is a special region with dynamic land cover and use changes due to human activity. Different from the upper HRB regions where climate change has been the controlling factor for hydrological and ecological processes, surface water condition is extremely important in the middle HRB where irrigated farmland is the largest land use and natural oases have been gradually replaced by artificial oases (Li et al., 2001, Cheng et al., 2014). According to our study, hydrological drought indices should be a better indicator than meteorological drought indices for water supply and demand conditions in the middle HRB. Zhang et al. (2014) found that the streamflow from the upper to middle HRB has risen due to climate change, but the streamflow from middle to lower HRB has reduced. They attributed this reduction to increasing water consumption by human activities in the middle HRB. Our study indicates less dryness trend in the middle HRB and therefore supports the analysis that climate change was not a major factor for the reduction. Sun et al. (2015) found an increasing trend in vegetation growth in the middle HRB and attributed it to irrigation. Our study shows less drought trend in this region, suggesting that more net water was another contributor to the increasing vegetation growth.

4.2 Importance of land-surface processes

The water shortage and frequent droughts are the biggest environmental threat to the ecosystems and human activities in the HRB as well as entire northwestern China. This comparison study provides evidence for the importance of water and energy interactions between land process and the atmosphere and between upstreams and downstreams in determining climate types in an arid climate. Because the *ESI* values are related to *AET* that is controlled by land-surface properties and management practices (e.g., rainfall-fed crops vs irrigated crops; natural wetlands vs cultivated drained croplands), our results suggest the land-surface processes play an important role in affecting drought conditions and their

variability. The landscape in the HRB, especially its transition zone, has changed remarkably in the past several decades due to urbanization, farming, and grazing activities (Hu et al., 2015). The irrigation may have caused the lower basin more water stressed (higher *ESI* than *AI*) since stream water from Heihe is intercepted and rivers go dry downstreams. The *ESI* should reflect this change since it is calculated partially based on the land-surface hydrological conditions. The regional land-atmosphere coupled models would provide proofs for this hypothesis though modeling the impacts of land cover change, which is a driver of local land-atmosphere interactions.

4.3 Role in moderating climate

The magnitude of *AI* (*ESI*) inter-annual variability in the middle basin is (in not) very close to that in the lower basin, another evidence for the unique capacity of *ESI* in separating the climate zones between the middle and lower basin reaches. The magnitude of the relative inter-annual variability differs mainly between *AI* and *ESI*, larger with *AI*. In addition, both *AI* and *ESI* in the HRB decreased dramatically from 1980 to 2010, at greater rate with *AI*. Thus, the drought conditions described using *ESI* is less variable, suggesting the role of local hydrological processes in moderating extreme climate events.

4.4 Future trends

One of the hydrological consequences from the projected climate change due to the greenhouse gas increase is more frequent and intense droughts in watersheds of dry regions. In the Colorado River Basin, global warming may lead to substantial water supply shortages (McCabe and Wolock, 2007), and the climate models projected considerably more drought activities in the 21st century (Cayan et al., 2010). In the HRB, the climate of the upper HRB will likely become warmer and wetter in the near future (Zhang et al., 2016), consistent with the historical records. Correspondingly the basin-wide evapotranspiration, snowmelt, and runoff are projected to increase over the same period. Many drought indices, including the *AI*, have been used to project future drought trends (Paulo et al., 2012). However, most of the recent *ESI* studies are based on historical remote sensing for monitoring short-term drought development, which limits the application of this drought index to climate change and drought impact research. Due to the unique ability with the *ESI* in identifying the transition

climate zone as shown in this study, it would be valuable to explore its potential for future drought projection study and compare with that of the *AI*.

4.5 Uncertainty and future research

The regional climate simulation which generated data for this analysis has many uncertainties (Xiong and Yan, 2013). One of the contributing factors is the very limited number of meteorological, hydrological, and ecological measurement sites. A large-scale, multiple-year field experiment project has been conducted in the HRB, which have been generating extensive datasets (Wang et al., 2014). These data are being used to improve the regional climate modeling, which will in turn generate new high-resolution data for further drought analysis. Furthermore, the regional climate modeling has been expanded into the middle 21st century, providing data for calculating the drought indices and comparing their future trends. Comparisons of other meteorological and hydrological drought indices are also a future research issue.

5 Conclusions

This study has found that the *ESI* climate classification agrees with the Koppen climate classification (Peel et al., 2007). By this system, we found that the climate types are different among the upper, middle, and lower HRB. In contrast, there would be no difference between the middle and lower HRB regions when the *AI* was used. The comparison results from this study therefore suggest that only *ESI* is able to identify a transition climate zone between the relatively humid climate in the mountains and the arid climate in the Gobi desert region. We conclude that the hydrological drought index *ESI* is a better index than the meteorological drought index *AI* for aridity classification in the HRB with a complex topography and land cover. Selection of the most appropriate drought index facilitates drought characterization, drought assessment and risk mitigation, and water resources management in the arid region.

Acknowledgement This study was supported by the National Natural Science Foundation of China (NSFC) (No. 91425301) and the USDA Forest Service. We thank the reviewer for valuable and insightful comments and suggestions.

References

- Allen, R. G., Pereira, L. S., Raes, D., and Smith, M.: “Crop evapotranspiration: guidelines for computing crop water requirements.” Irrigation and Drainage Paper No. 56, Food and Agriculture Organization of the United Nations, Rome, Italy, 1998.
- Anderson, M. C., Hain, C. R., Wardlow, B., Mecikalski, J. R., and Kustas, W. P.: Evaluation of drought indices based on thermal remote sensing of evapotranspiration over the continental U.S. *Journal of Climate*, 24, 2025–2044, 2011.
- Anderson, M. C., Zolin, C. A., Sentelhas, P. C., Hain, C. R., Semmens, K., Yilmaz, M. T., Gao, F., Otkin, J. A., and Tetrault, R.: The Evaporative Stress Index as an indicator of agricultural drought in Brazil: An assessment based on crop yield impacts, *Remote Sensing of Environment*, 174, 82–99, doi:10.1016/j.rse.2015.11.034, 2016.
- Arora, V. K.: The use of the aridity index to assess climate change effect on annual runoff, *Journal of Hydrology*, 265, 164–177, 2002.
- Budyko, M. I.: *Climate and Life*, Academic, San Diego, CA, 508 pp., 1974.
- Cayan, D. R., Das, T., Pierce, D. W., Barnett, T. P., Tyree, M., and Gershunov, A.: Future dryness in the southwest US and the hydrology of the early 21st century drought, *Proc. Natl. Acad. Sci.*, 107, 21, 271–21, 276. <http://research001.com/?showinfo-140-577279-0.html>, 2010.
- Chen, Y., Zhang, D., Sun, Y., Liu, X., Wang, N., and Savenije, H.: Water demand management: A case study of the Heihe River Basin in China. *Phys. Chem. Earth*, 30, 408–419, <http://dx.doi.org/10.1016/j.pce.2005.06.019>, 2005.
- Cheng, G.D., Li, X., Zhao, W.Z., Xu, Z.M., Feng, Q., Xiao, S.C., Xiao, H.L.: Integrated study of the water–ecosystem–economy in the Heihe River Basin, *National Science Review*, 1: 413–428, doi: 10.1093/nsr/nwu017, 2014.
- Choi, M., Jacobs, J. M., Anderson, M. C., and Bosch, D. D.: Evaluation of drought indices via remotely sensed data with hydrological variables, *Journal of Hydrology*, 476, 265–273. doi:10.1016/j.jhydrol.2012.10.042, 2013.
- Gao, B., Qin, Y., Wang, Y. H., Yang, D., and Zheng, Y.: Modeling Ecohydrological Processes and Spatial Patterns in the Upper Heihe Basin in China, *Forests*, 7(1). doi:10.3390/f7010010, 2016.

542 Guttman, N.B.: Accepting the standardized precipitation index: a calculation algorithm.
 543 JAWRA Journal of the American Water Resources Association, John Wiley & Sons, 35
 544 (2): 311–322. doi:10.1111/j.1752-1688.1999.tb03592.x. 1999.

545 Hamon, W. R.: Computation of direct runoff amounts from storm rainfall. Intl. Assoc.
 546 Scientific Hydrol. Publ., 63, 52- 62, 1963.

547 Hu, X., Lu, L., Li, X., Wang, J., and Guo, M.: Land use/cover change in the middle reaches
 548 of the Heihe River Basin over 2000-2011 and its implications for sustainable water
 549 resource management. PLoS ONE 10(6): e0128960. doi:10.1371/journal.pone.0128960,
 550 2015.

551 Keetch, J.J., Byram, G.M.: A drought index for forest fire control. USDA Forest Service
 552 Research Paper No. SE38, pp. 1–32.1968.

553 Li, J.: Multivariate Frequencies and Spatial Analysis of Drought Events Based on
 554 Archimedean Copulas Functio, Northwest University of Science and Technology, 2012.

555 Li, X., Lu, L, Cheng, G.D., Xiao, H.L.: Quantifying landscape structure of the Heihe River
 556 Basin, north-west China using FRAGSTATS, Journal of Arid Environments, 48: 521–535,
 557 doi:10.1006/jare.2000.0715, 2001.

558 McCabe, G. J., and Wolock, D. M.: Warming may create substantial water supply shortages
 559 in the Colorado River basin, Geophysical Research Letters, 34, 22, 2007.

560 McKee, T.B., Doesken, N.J., Kleist, J.: The Relationship of Drought Frequency and Duration
 561 to Time Scales. Proceedings of the Eighth Conference on Applied Climatology. American
 562 Meteorological Society: Boston; 179–184, 1993.

563 Nalbantis, I. and Tsakiris, G. Assessment of hydrological drought revisited Water Resour.
 564 Manag. 23 881–97, 2009.

565 Narasimhan, B., and Srinivasan, R.: Development and evaluation of soil moisture deficit
 566 index and evapotranspiration deficit index for agricultural drought monitoring.
 567 Agricultural and Forest Meteorology, 133, 69-88. 2005.

568 Onder, D., Aydin M., Berberoglu, S., Onder, S., and Yano, T.: The use of aridity index to
 569 assess implications of climatic change for land cover in Turkey. Turkish Journal of
 570 Agriculture and Forestry, 33, 305-314, 2009.

- Otkin, J. A., Anderson, M. C., Hain, C. R., Mladenova, I. E., Basara, J. B., and Svoboda, M.: Examining rapid onset drought development using the thermal infrared based Evaporative Stress Index, *Journal of Hydrometeorology*, 14, 1057–1074, 2013.
- Palmer, W.C.: Meteorological drought. U.S. Research Paper No. 45. US Weather Bureau, Washington, DC, <https://www.ncdc.noaa.gov/temp-and-precip/drought/docs/palmer.pdf>, 1965.
- Paulo, A. A., Rosa, R. D., and Pereira, L. S.: Climate trends and behavior of drought indices based on precipitation and evapotranspiration in Portugal, *Nat. Hazards Earth Syst. Sci.*, 12, 1481–1491, 2012.
- Peel, M. C., Finlayson, B. L., and McMahon, T. A.: Updated world map of the Köppen–Geiger climate classification. *Hydrol. Earth Syst. Sci.*, 11, 1633–1644. doi:10.5194/hess-11-1633-2007, 2007.
- Ponce, V. M., Pandey, R. P., and Ercan, S.: Characterization of drought across climatic spectrum. *Journal of Hydrologic Engineering, ASCE* 5, 222–2245, 2000.
- Ren, Z., Lu, Y., and Yang, D.: Drought and flood disasters and rebuilding of precipitation sequence in Heihe River basin in the past 2000 years, *J. Arid Land Resour. Environ.*, 24, 91–95, 2010.
- Shukla, S., and Wood, A.W.: Use of a standardized runoff index for characterizing hydrologic drought. *Geophys. Res. Lett.*, 35, L02405. doi:10.1029/2007GL03248. 2008.
- Sun, W., Song, H., Yao, X., Ishidaira, H., Xu, Z.: Changes in remotely sensed vegetation growth trend in the Heihe basin of arid northwestern China. *PLoS ONE*, 10(8): e0135376. doi:10.1371/journal.pone.0135376, 2015.
- Svoboda, M., LeComte, D., Hayes, M., Heim, R., Gleason, K., Angel, J., Rippey, B., Tinker, R., Palecki, M., Stooksbury, D., Miskus, D., and Stephin, S.: The Drought Monitor, *Bulletin of the American Meteorological Society*, 83, 1181-90, 2002.
- UNESCO, Map of the World Distribution of Arid Regions. MAB Techn. Note 7, 1979.
- Wolfe, S. A.: Impact of increased aridity on sand dune activity in the Canadian Prairies. *Journal of Arid Environments*, 36, 421-432, 1997.
- Wang, L. X., Wang, S. G., and Ran, Y. H.: Data sharing and data set application of watershed allied telemetry experimental research, *IEEE Geoscience and Remote Sensing Letters*, 11, 2020-2024, 10.1109/LGRS.2014.2319301, 2014.

- Wilhite, D. A. and Glantz, M. H.: Understanding the drought phenomenon: The role of definitions. *Water International* 10:111–20. 1985.
- Woodhouse, C. A., Meko, D. M., MacDonald, G. M., Stahle, D. W., and Cook, E. R.: A 1,200-year perspective of 21st century drought in southwestern North America. *Proc. Natl. Acad. Sci. USA*, 107, 21283–21288, 2010.
- Xiong, Z., and Yan, X. D.: Building a high-resolution regional climate model for the Heihe River Basin and simulating precipitation over this region. *Chin. Sci. Bull*, 58, 4670–4678, doi: 10.1007/s11434-013-5971-3, 2013.
- Yang, D. W., Gao, B., Jiao, Y., Lei, H. M., Zhang, Y. L., Yang, H. B., and Cong, Z. T.: A distributed scheme developed for eco-hydrological modeling in the upper Heihe River. *Sci. China Earth Sci.*, 58, 36–45. <http://dx.doi.org/10.1007/s11430-014-5029-7>, 2015.
- Yang, G. H.: *Agricultural Resources and Classification*, China Agricultural Press, Beijing, China, 286 pp., 2007.
- Yao, A. Y. M.: Agricultural potential estimated from the ratio of actual to potential evapotranspiration, *Agricultural Meteorology*, 13, 405–417, doi: 10.1016/0002-1571(74)90081-8, 1974.
- Zhang, A. J., Liu, W. B., Yin, Z. L., Fu, G. B., and Zheng, C. M.: How will climate change affect the water availability in the Heihe River Basin, Northwest China? *J. Hydrometeorology*, doi: <http://dx.doi.org/10.1175/JHM-D-15-0058.1>, 2016.
- Zargar, A., Sadiq, R., Naser, B., and Khan, F. I.: A review of drought indices. *Environmental Reviews*, 19, 333–349. 2011.
- Zhang, A.J., Zheng, C.M., Wang, S., Yao, Y.Y.: Analysis of streamflow variations in the Heihe River Basin, northwest China: Trends, abrupt changes, driving factors and ecological influences, *Journal of Hydrology: Regional Studies* 3, 106–124, 2015.